Open access • Journal Article • DOI:10.1063/1.3187803

Mobility oscillation by one-dimensional quantum confinement in Si-nanowire metal-oxide-semiconductor field effect transistors — Source link

Hironori Yoshioka, Naoya Morioka, Jun Suda, Tsunenobu Kimoto

Published on: 13 Aug 2009 - Journal of Applied Physics (American Institute of Physics)

Topics: Upper hybrid oscillation, Transconductance, Fermi level, Effective mass (solid-state physics) and MOSFET

Mobility oscillation by one-dimensional quantum confinement in Si-nanowire metal-oxide-semiconductor field effect transistors

AUTHOR(S):

Yoshioka, Hironori; Morioka, Naoya; Suda, Jun; Kimoto, Tsunenobu

JOURNAL OF APPLIED PHYSICS **106**, 034312 (2009)

Mobility oscillation by one-dimensional quantum confinement in Si-nanowire metal-oxide-semiconductor field effect transistors

Hironori Yoshioka,[1,a)] Naoya Morioka,[1] Jun Suda,[1] and Tsunenobu Kimoto[1,2]
[1]*Department of Electronic Science and Engineering, Kyoto University, Kyoto 615-8510, Japan*
[2]*Photonics and Electronics Science and Engineering Center, Kyoto University, Kyoto 615-8510, Japan*

(Received 9 June 2009; accepted 22 June 2009; published online 13 August 2009)

Si-nanowire *p*-channel metal-oxide-semiconductor field effect transistors (MOSFETs), in which the typical cross section of the nanowire is a rectangular shape with 3 nm height and 18 nm width, have been fabricated and the current-voltage characteristics have been measured from 101 to 396 K. The transconductance has shown oscillation up to 309 K. The carrier transport has been theoretically analyzed, assuming that the acoustic phonon scattering is dominant. The electronic states have been determined from the effective mass approximation and the mobility from the relaxation time approximation as a function of the Fermi level. Relation between the gate voltage and the Fermi level has been estimated from the MOSFET structure. The calculated mobility has shown the oscillation with change in the Fermi level (the gate voltage), resulting in the transconductance oscillation. The oscillation originates from one-dimensional density of states ($\propto E^{-0.5}$). © *2009 American Institute of Physics*. [DOI: 10.1063/1.3187803]

I. INTRODUCTION

Si complementary metal-oxide-semiconductor (CMOS) technology has been making great progress due to the scalability of the metal-oxide-semiconductor field effect transistors (MOSFETs). However, further scaling will not be easy in the future because of fundamental problems,[1–3] and new materials or new device structures are intensively needed. MOSFETs using a new gate geometry such as fin MOSFETs (Ref. 4) and gate-around MOSFETs[5–9] are one of the most promising candidates for breaking the limits of conventional devices because they can effectively suppress the short-channel effects.[4–10] The cross sectional size of the channel will be further reduced and will reach several nanometers (nanowire) to get even better gate controllability.

In the nanowires, the carriers are confined in the perpendicular direction to the electrical conduction by the electric potential, and one-dimensional electronic transport may be expected. The conduction and valence bands are divided into subbands, and the density of states (DOS) consists of superposition of each subband's DOS, which is proportional to $E^{-0.5}$. The DOS, therefore, shows oscillation with change in the electron energy.[11,12] By the subband splitting, the decrease in the conductivity effective mass or intervalley scattering, both of which result in the increase in the mobility, is expected.[13] Therefore, it is important to clarify the subband splitting and its effect on the transport characteristics.

Oscillation in the drain current with the gate voltage at low drain voltage (V_{DS}=0.2 mV) below 28 K for trigate MOSFETs with the fin width and height of 45 and 82 nm, respectively, has been reported.[11,14] Similar oscillation has also been reported at higher drain voltage (V_{DS}=50 mV) and higher temperature ($\leq$137 K) for ~7 nm triangular gate all around MOSFETs.[12] It has been explained that the dip of the drain current is due to the intersubband scattering and to the limited increase in the electron concentration with the gate voltage when the first subband is almost filled but the second subband is still empty. However, a quantitative analysis has not been made, and the origin of the oscillation has not been revealed yet.

In this study, Si-nanowire MOSFETs have been fabricated and characterized. The transconductance has shown clear oscillation at temperature up to 309 K. The carrier transport in the Si-nanowire has been analyzed, assuming that the acoustic phonon scattering is dominant. The calculation has indicated that the oscillation originates from the periodic variations in the scattering rate caused by one-dimensional DOS ($\propto E^{-0.5}$).

II. DEVICE FABRICATION

Figure 1 illustrates the schematic structure of Si-nanowire MOSFETs fabricated in this study. The starting material was Si on insulator with the top Si (001) layer being 40 nm thick, which was thinned by sacrificial oxidation at

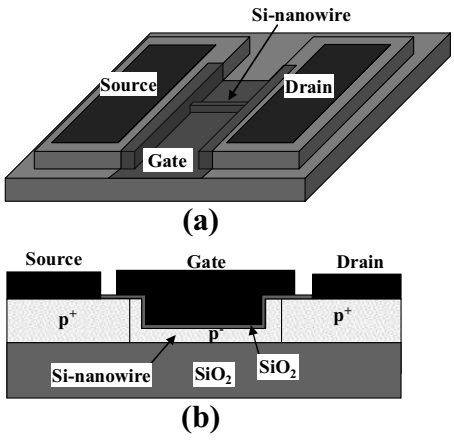

FIG. 1. Schematic structure of a fabricated Si-nanowire MOSFET. (a) A bird's eye view and (b) a cross section parallel to the nanowire.

a)Electronic mail: yoshioka@semicon.kuee.kyoto-u.ac.jp.

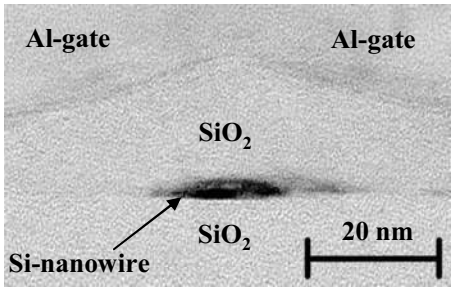

FIG. 2. Cross sectional TEM images of fabricated nanowire MOSFET. The cross section of the nanowire was nearly rectangular with 3 nm height and 18 nm width.

1150 °C, with a high resistivity of 5–50 Ω cm (p-type). The nanowire shape was formed by using electron beam lithography and reactive ion etching (RIE). The nanowire length was 100 nm and the direction was [100]. The source/drain regions were formed by B^+ implantation at 7 keV with a dose of 2×10^{14} cm^{-2}. To remove the RIE damage and to reduce the nanowire size, sacrificial oxidation was carried out at 1000 °C for 10 min in dry O_2. The gate insulator of SiO_2 was subsequently formed by dry oxidation at 1000 °C for 10 min. The thickness of the gate SiO_2 was about 19 nm. Al was employed for the source/drain and gate electrodes. Contact annealing was carried out in the forming gas at 350 °C for 10 min.

Figure 2 shows the cross sectional transmission electron microscopy (TEM) image of a fabricated nanowire MOSFET. The cross section of the nanowire was nearly rectangular with 3 nm height and 18 nm width.

III. EXPERIMENTAL RESULTS

Figure 3 shows the drain current (I_{DS}) versus gate voltage (V_{GS}) characteristics and Fig. 4 shows the transconductance (g_m) versus gate voltage (V_{GS}) characteristics at various temperatures. Both figures show characteristics for the p-channel Si-nanowire MOSFET shown in Fig. 2. The temperature was changed from 101 to 396 K, and the drain voltage was fixed at −50 mV. The substrate voltage was fixed at 0 V for all the electrical measurements. At the high gate voltage, the drain current increased with the decrease in temperature, indicating that the phonon scattering is dominant. Significant oscillation of the transconductance was observed at 101 K. The magnitude of the oscillation becomes smaller with increasing temperature, but clear oscillation can be still seen at 309 K. The gate voltages of local maxima/minima for the transconductance showed very little change with temperature change.

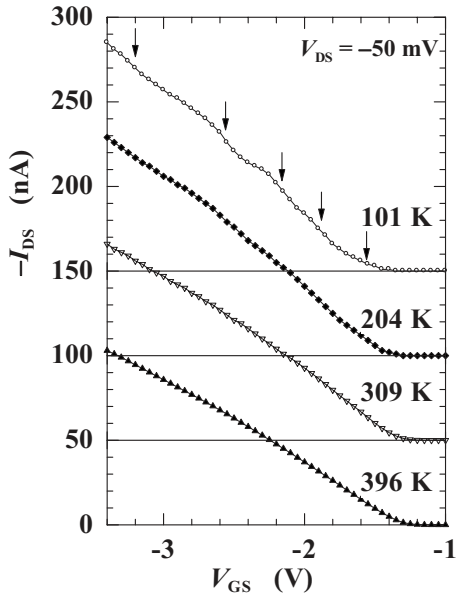

FIG. 3. Gate characteristics of the Si-nanowire MOSFET shown in Fig. 2. The temperature was changed from 101 to 396 K, and the drain voltage was fixed at −50 mV. The drain currents are shift by 50 nA for every measured temperature. The arrows show peaks of the slope.

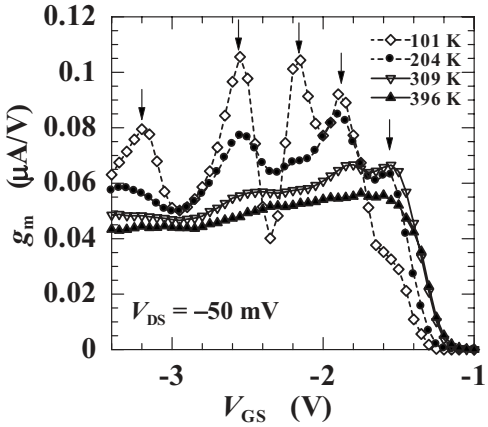

FIG. 4. Gate voltage dependence of transconductance g_m of the Si-nanowire MOSFET shown in Fig. 2. The temperature was changed from 101 to 396 K, and the drain voltage was fixed at −50 mV. The arrows show peaks of oscillation.

IV. THEORETICAL MODEL

To explain the oscillation of the transconductance, a theoretical model for the carrier transport in the Si-nanowire MOSFETs is proposed in this chapter. The mobility is determined by carrier scattering, assuming the carriers to be confined in a one-dimensional nanowire. Then, to obtain the transconductance, the dependence of the carrier concentration and mobility on the gate voltage is calculated.

For simplicity, the mobility determined by the longitudinal acoustic phonon scattering is considered, and it is assumed that the phonon states in the nanowire are the same as those in bulk.[15] The displacement of atoms at the position $\boldsymbol{r}$ is given by[16]

$$\boldsymbol{u} = \sum_{\boldsymbol{\beta}} \sqrt{\frac{\hbar}{2\rho\Omega\omega_{\boldsymbol{\beta}}}}\boldsymbol{e}_{\boldsymbol{\beta}}[a_{\boldsymbol{\beta}}\exp(i\boldsymbol{\beta}\cdot\boldsymbol{r}) + a_{\boldsymbol{\beta}}^{\dagger}\exp(-i\boldsymbol{\beta}\cdot\boldsymbol{r})] \quad (1)$$

and the scattering potential by[17]

$$U = D_A\frac{\partial}{\partial\boldsymbol{r}}\cdot\boldsymbol{u}, \quad (2)$$

where $\rho(2.33\times10^3\ kg/m^3)$ is the mass density of Si lattice, Ω is the bulk volume, $\boldsymbol{\beta}$ is the wave number vector of phonons, $\omega_{\boldsymbol{\beta}}$ is the angular frequency of phonons, $\boldsymbol{e}_{\boldsymbol{\beta}}$ is the unit vector which is parallel to $\boldsymbol{u}$, $a_{\boldsymbol{\beta}}$ and $a_{\boldsymbol{\beta}}^{\dagger}$ are the creation

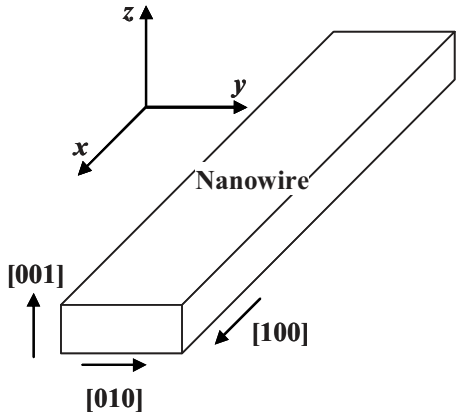

FIG. 5. Shape and crystalline orientations of the nanowire and the coordinate axes for calculation. The nanowire is rectangular in cross section.

and annihilation operators of phonons, respectively, and D_A (5.0 eV for holes) is the acoustic deformation potential.[18]

It is assumed that the nanowire is rectangular in the cross section. The crystalline orientations and the coordinate axes are set, as shown in Fig. 5. The Schrödinger equation with the effective mass approximation is used to describe the wave function in the nanowire. The infinite quantum well of width W_y and W_z in the y- and z-directions, respectively, and infinitely large width W_x in the x-direction are assumed. For the holes, two valence band maxima, whose constant energy surfaces in the momentum space are approximated as the spheres with the heavy-hole effective mass $m*_H$ $(0.49m_0)$ and with the light-hole effective mass $m*_L$ $(0.16m_0)$, are considered (m_0 is the electron mass). For simplicity, the scattering between the heavy-hole and light-hole bands is ignored. The solution of the Schrödinger equation is given by

$$\psi_{\boldsymbol{k}} = \frac{1}{\sqrt{W_x}}\exp(ik_x x)\sqrt{\frac{2}{W_y}}\sin(k_y y)\sqrt{\frac{2}{W_z}}\sin(k_z z), \tag{3}$$

$$E_{\boldsymbol{k}} = E_{k_x} + E_{k_y} + E_{k_z}, \tag{4}$$

where

$$E_{k_l} \equiv -\frac{\hbar^2 k_l^2}{2m*_l}, \tag{5}$$

$$k_x = \frac{2\pi n_x}{W_x} \quad (n_x = 0, \pm 1, \pm 2, \ldots), \tag{6}$$

$$k_j = \frac{\pi n_j}{W_j} \quad (n_j = 1, 2, \ldots), \tag{7}$$

for $l=x,y,z$ and $j=y,z$, where $m*_l$ is the effective mass and the energy of the valence-band maxima of bulk is fixed at zero. The DOS is given by

$$g(E) = \sum_{k_y,k_z} g_{k_y,k_z}(E) \tag{8}$$

as the sum of the one-dimensional DOSs of subbands labeled k_y, k_z

$$g_{k_y,k_z}(E) = \frac{1}{W_y W_z}\frac{1}{\pi\hbar}\sqrt{\frac{2m*_x}{-E + E_{k_y} + E_{k_z}}}. \tag{9}$$

The nonzero matrix elements of the scattering potential between the states $\boldsymbol{k}'$ and $\boldsymbol{k}$ are obtained from Eqs. (2) and (3) by[17]

$$\begin{aligned} M(\boldsymbol{k}', \boldsymbol{k}, \pm\boldsymbol{\beta}) &\equiv \langle \boldsymbol{k}'; N_{\boldsymbol{\beta}_1}, N_{\boldsymbol{\beta}_2}, \ldots, N_{\boldsymbol{\beta}} \mp 1, \ldots \\ &\quad \times |U| \boldsymbol{k}; N_{\boldsymbol{\beta}_1}, N_{\boldsymbol{\beta}_2}, \ldots, N_{\boldsymbol{\beta}}, \ldots \rangle \\ &= \sqrt{\frac{\hbar}{2\rho\Omega\omega_{\boldsymbol{\beta}}}} D_A(\pm|\boldsymbol{\beta}|i)\sqrt{N_{\boldsymbol{\beta}} + 1/2 \mp 1/2} \\ &\quad \times I_{k'_y,k_y}(\beta_y) I_{k'_z,k_z}(\beta_z), \end{aligned} \tag{10}$$

where

$$k'_x = k_x \pm \beta_x \ \text{(momentum conservation)}, \tag{11}$$

$$I_{k'_j,k_j}(\beta_j) \equiv \int_0^{W_j} \frac{2}{W_j}\sin(k'_j j)\sin(k_j j)\exp(\pm i\beta_j j)dj \tag{12}$$

for $j=y, z$. Here, the upper/lower of the double sign corresponds to absorption/emission of one phonon of the state $\boldsymbol{\beta}$, and $N_{\boldsymbol{\beta}}$ is the number of phonons of the state $\boldsymbol{\beta}$. The transition rate from the state $\boldsymbol{k}$ to $\boldsymbol{k}'$ by the absorption/emission of the phonon $\boldsymbol{\beta}$ is taken from Fermi's golden rule and Eq. (10) (Ref. 17)

$$S(\boldsymbol{k}', \boldsymbol{k}, \pm\boldsymbol{\beta}) = \frac{2\pi}{\hbar}|M(\boldsymbol{k}', \boldsymbol{k}, \pm\boldsymbol{\beta})|^2 \delta(E_{\boldsymbol{k}'} - E_{\boldsymbol{k}} \mp \hbar\omega_{\boldsymbol{\beta}}). \tag{13}$$

The inverse of the relaxation time of the state $\boldsymbol{k}$ is given by summing the transition rate over all the final states, using the relaxation time approximation assuming that the phonon scattering is elastic and isotropic[17]

$$1/\tau(\boldsymbol{k}) = \sum_{\boldsymbol{k}',\parallel} \sum_{\pm} \sum_{\beta_y,\beta_z} S(\boldsymbol{k}', \boldsymbol{k}, \pm\boldsymbol{\beta}), \tag{14}$$

where the summation over "±" represents the sum of the absorption and emission, and "$\boldsymbol{k}'$, ∥" represents the sum over the states $\boldsymbol{k}'$ whose spin is parallel to that of the initial state $\boldsymbol{k}$. Furthermore, the following approximations were used to work out Eq. (14):

$$N_{\boldsymbol{\beta}} + 1/2 \mp 1/2 = \frac{1}{\exp(\hbar\omega_{\boldsymbol{\beta}}/kT) - 1} + 1/2 \mp 1/2 \approx \frac{kT}{\hbar\omega_{\boldsymbol{\beta}}}, \tag{15}$$

$$E_{\boldsymbol{k}'} - E_{\boldsymbol{k}} \mp \hbar\omega_{\boldsymbol{\beta}} \approx E_{\boldsymbol{k}'} - E_{\boldsymbol{k}}, \tag{16}$$

$$\omega_{\boldsymbol{\beta}} \approx v_P \beta, \tag{17}$$

where v_P is the velocity of the longitudinal acoustic phonon $(9.04\times10^3$ m/s[10,11]). Equation (14) then results in[17]

$$1/\tau(\boldsymbol{k}) = C\sum_{k'_y,k'_z} g_{k'_y,k'_z}(E)(1+1/2\,\delta_{k'_y,k_y})(1+1/2\,\delta_{k'_z,k_z}), \quad (18)$$

where

$$C \equiv \frac{\pi {D_A}^2 kT}{\hbar {v_P}^2 \rho}. \quad (19)$$

To determine $1/\tau(\boldsymbol{k})$ as a function of the energy E, we assumed the Kronecker's δ to be united in Eq. (18). Then, Eq. (18) can be simplified to

$$1/\tau(\boldsymbol{k}) \approx 1/\tau(E) \equiv C\sum_{k'_y,k'_z} g_{k'_y,k'_z}(E)\cdot\frac{9}{4}. \quad (20)$$

Although this approximation overestimates the contribution to $1/\tau(\boldsymbol{k})$ by the intersubband scattering, it may be reasonable for small nanowires, in which the subband splitting is so large that the DOSs of the subbands hardly overlap with each other.

The carrier concentration in the nanowire is given by

$$p(E_F) = \frac{1}{W_x W_y W_z}\sum_{\boldsymbol{k}} f = \int_{-\infty}^{0} g(E) f dE \quad (21)$$

as a function of the Fermi level E_F, where f is the Fermi distribution function expressed by

$$f = \frac{1}{1+e^{(-E+E_F)/kT}}. \quad (22)$$

The average relaxation time for the energy E is given from the Boltzmann's transport equation as[17]

$$\langle\tau\rangle(E_F) = \frac{\sum_{\boldsymbol{k}} \frac{2E_{k_x}}{kT}\tau(E) f(1-f)}{\sum_{\boldsymbol{k}} f} = \frac{\sum_{k_y,k_z}\int_{-\infty}^{0} g_{k_y,k_z}(E)\frac{2(-E+E_{k_y}+E_{k_z})}{kT}\tau(E) f(1-f) dE}{p(E_F)}, \quad (23)$$

and the mobility can be calculated by

$$\mu(E_F) = \frac{e\langle\tau\rangle(E_F)}{m*_x}. \quad (24)$$

After determining $p(E_F)$ and $\mu(E_F)$ of each band maximum as a function of E_F, the total carrier concentration and the average mobility are obtained as follows:

$$p = \sum_m p_m, \quad (25)$$

$$\mu = \frac{1}{p}\sum_m p_m \mu_m, \quad (26)$$

where the index m labels the heavy-hole and light-hole bands.

On the other hand, the gate voltage is given by[19]

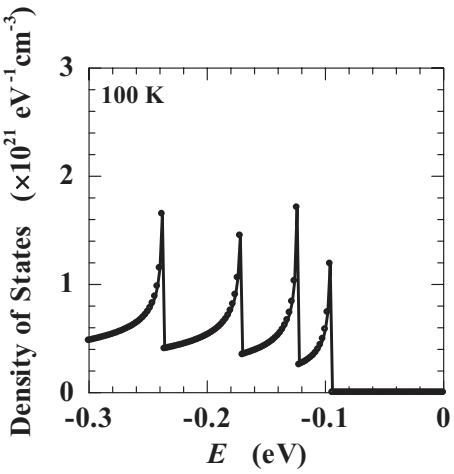

(a)

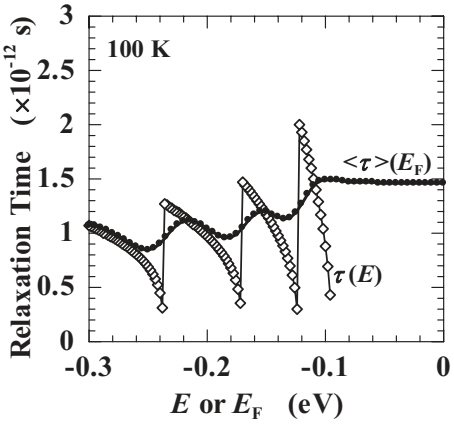

(b)

FIG. 6. (a) Calculated DOS $g(E)$ and (b) relaxation time $\tau(E)$ vs E and average relaxation time $\langle\tau\rangle(E_F)$ vs E_F with W_y=9 nm and W_z=3 nm at 100 K.

$$V_{GS} - V_{FB} = V_{OX} + \frac{1}{e}(E_F - E_{F0}), \quad (27)$$

where V_{FB} is the flatband voltage, E_{F0} is the Fermi level in the nanowire at $V_{GS}-V_{FB}=0$, and

$$V_{OX} = -\frac{epW_yW_z}{C_{OX}}. \quad (28)$$

The gate SiO_2 capacitance C_{OX} per unit length of the nanowire was calculated by solving the two-dimensional Poisson's equation using the structural data measured from the TEM images in Fig. 2. The calculation was carried out by using a device simulator, where the dielectric constant ε_{OX} of the gate SiO_2 was $3.9\varepsilon_0$. The calculated C_{OX} was 1 pF/cm. In the actual calculation for any size of nanowires, C_{OX} was fixed at 1 pF/cm. Equation (27) is transformed into

$$V'_{GS}(E_F) \equiv V_{GS} - V_{FB} + \frac{1}{e}E_{F0} = V_{OX} + \frac{1}{e}E_F. \quad (29)$$

Thus, $V'_{GS}(E_F)$ can be determined as a function of E_F, and the carrier concentration p and mobility μ, therefore, can be determined as a function of V'_{GS} through E_F.

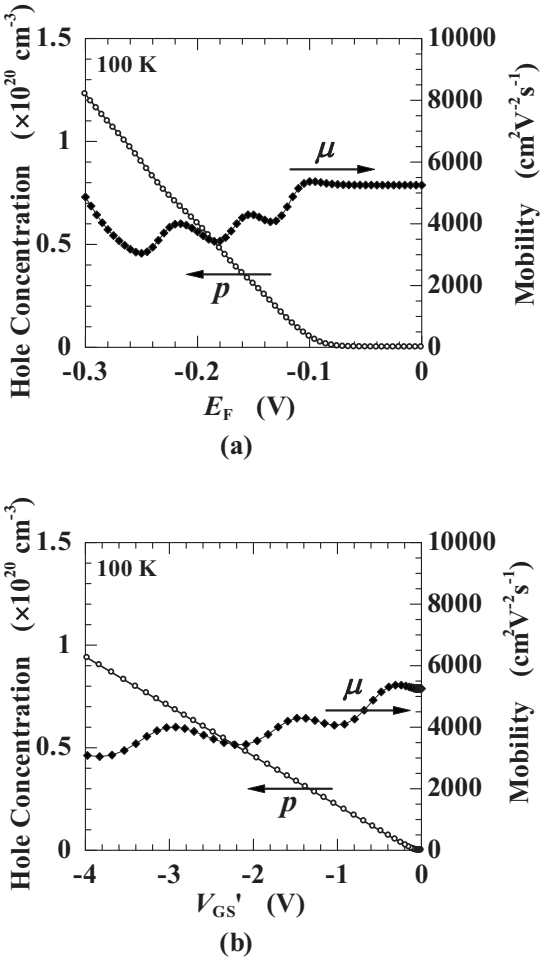

FIG. 7. Calculated carrier concentration p and mobility μ vs (a) E_F and (b) V'_{GS} with W_y=9 nm and W_z=3 nm at 100 K.

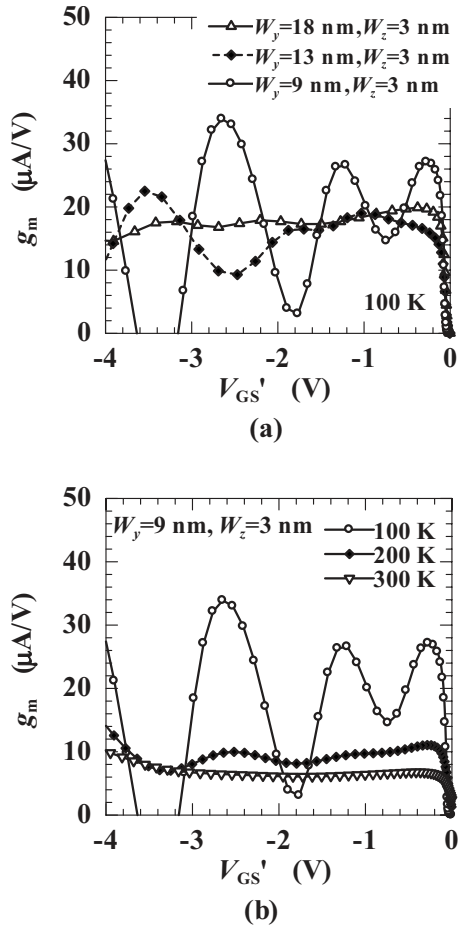

FIG. 8. Calculated transconductance g_m vs V'_{GS} for MOSFETs, (a) with different nanowire sizes at 100 K, and (b) with nanowire size of W_y =9 nm and W_z=3 nm at different temperatures.

V. CALCULATED RESULTS AND DISCUSSION

Figure 6 shows the calculated (a) DOS $g(E)$ versus E, and (b) relaxation time $\tau(E)$ versus E and average relaxation time $\langle\tau\rangle(E_F)$ versus E_F with W_y=9 nm and W_z=3 nm (9, 3) at 100 K. The relaxation time is in inverse proportion to $g(E)$ according to Eq. (20), and $\langle\tau\rangle(E_F)$ is almost the average of $\tau(E)$ at around $E=E_F$. Then, the average relaxation time oscillates because of the oscillation of DOS. For instance, the decrease in $\langle\tau\rangle(E_F)$ near −0.12 eV originates from the increase in DOS by the second subband, namely, from the increase in both intersubband scattering from the first to second subband and intrasubband scattering from the second to second.

Figure 7 shows the calculated carrier concentration p and mobility μ versus (a) E_F and (b) V'_{GS} with (9, 3) at 100 K. The linear dependence of the carrier concentration on V'_{GS} is reasonable because p changes with the change in V'_{GS}, obeying an approximated equation

$$dV'_{GS}(E_F) \approx -\frac{eW_yW_z}{C_{OX}}dp \tag{30}$$

at high concentration and high temperature. On the other hand, the mobility, which is in proportion to $\langle\tau\rangle(E_F)$, shows clear oscillation with change in E_F or V'_{GS}.

The calculated transconductance (g_m) is plotted as a function of V'_{GS} in Fig. 8. The magnitude of the oscillation increases with the decrease in temperature or nanowire size. The peak positions of the oscillation are unchanged with temperature change. These results show agreement with the experimental results. At 100 K, the nanowire size of W_y =18 nm and W_z=3 nm (18, 3), which is the same size of the experiment, is not small enough to show the oscillation and smaller size such as (9, 3) is needed. Because the boundary of the nanowire was not clear in the TEM image (Fig. 2), the actual size of the nanowire may be smaller than (18, 3). The period of the oscillation was about 0.4 V in the experiment and about 1.2 V in the calculation for (9, 3). The assumption of the infinite quantum well overestimates the energy of the subband splitting, and the simplified symmetrical band structure underestimates the number of subbands. These factors may be the reason why the experimental period of the oscillation is smaller than the calculated period. At 100 K, maximum/minimum ratio of the oscillation in the experiment (about 2) is smaller than that in the calculation [about 3 for (9, 3)]. However, at 300 K, the experimental maximum/minimum ratio is larger than the calculation.

The kinks of the drain current at 101 K are similar to those reported in Ref. 12, where the cross sectional size of the nanowire is similar. The oscillation observed in this study

may be, therefore, the same phenomenon as that in Ref. 12. It is not clear in Ref. 12 whether the oscillational characteristics were observed at room temperature because the transconductance is not shown. The oscillational characteristics may be very small at room temperature and can only be observed in the transconductance. Measurements under reduced noise condition have enabled us to observe oscillational characteristics even at room temperature. Si-nanowire *n*-channel MOSFETs were also fabricated and showed similar oscillation to the *p*-channel MOSFET.

VI. CONCLUSIONS

Si-nanowire *p*-channel MOSFETs, in which the cross section of the nanowire is a rectangular shape with a height of 3 nm and width of 18 nm, were fabricated and the transconductance showed an oscillation up to 309 K. The oscillation may appear as a result of one-dimensional quantum confinement effects. To reveal the physical origin of the oscillation, a theoretical model for the carrier transport in the Si-nanowire MOSFETs was proposed. The calculation showed similar oscillation to the experiment. From the theoretical model, it is indicated that the oscillation originates from the periodic variations in the mobility (scattering rate) caused by one-dimensional DOS ($\propto E^{-0.5}$).

ACKNOWLEDGMENTS

The authors would like to thank Mr. Eiji Ohmura of Kyoto-Advanced Nanotechnology Network, Kyoto University for supporting us in the device fabrication process of electron beam lithography. This work was supported by the Global COE Program (C09) from the Ministry of Education, Culture, Sports, Science and Technology, Japan.

[1] W. Haensch, E. J. Nowak, R. H. Dennard, P. M. Solomon, A. Bryant, O. H. Dokumaci, A. Kumar, X. Wang, J. B. Johnson, and M. V. Fischetti, IBM J. Res. Dev. **50**, 339 (2006).
[2] D. J. Frank, R. H. Dennard, E. Nowak, P. M. Solomon, Y. Taur, and H.-S. P. Wong, Proc. IEEE **89**, 259 (2001).
[3] R. W. Keyes, Rep. Prog. Phys. **68**, 2701 (2005).
[4] X. Huang, W. -C. Lee, C. Kuo, D. Hisamoto, L. Chang, J. Kedzierski, E. Anderson, H. Takeuchi, Y. -K. Choi, K. Asano, V. Subramanian, T. -J. King, J. Bokor, and C. Hu, IEEE Trans. Electron Devices **48**, 880 (2001).
[5] N. Singh, A. Agarwal, L. K. Bera, T. Y. Liow, R. Yang, S. C. Rustagi, C. H. Tung, R. Kumar, G. Q. Lo, N. Balasubramanian, and D. -L. Kwong, IEEE Electron Device Lett. **27**, 383 (2006).
[6] Y. Cui, Z. Zhong, D. Wang, W. U. Wang, and C. M. Lieber, Nano Lett. **3**, 149 (2003).
[7] H. Majima, H. Ishikuro, and T. Hiramoto, IEEE Electron Device Lett. **21**, 396 (2000).
[8] V. Pott, K. E. Moselund, D. Bouvet, L. D. Michielis, and A. M. Ionescu, IEEE Trans. Nanotechnol. **7**, 733 (2008).
[9] K. H. Cho, S. D. Suk, Y. Y. Yeoh, M. Li, K. H. Yeo, D.-W. Kim, D. Park, W. -S. Lee, Y. C. Jung, B. H. Hong, and S. W. Hwang, IEEE Electron Device Lett. **28**, 1129 (2007).
[10] G. Pei, J. Kedzierski, P. Oldiges, M. Ieong, and E. C.-C. Kan, IEEE Trans. Electron Devices **49**, 1411 (2002).
[11] J.-P. Colinge, A. J. Quinn, L. Floyd, G. Redmond, J. C. Alderman, W. Xiong, C. R. Cleavelin, T. Schulz, K. Schruefer, G. Knoblinger, and P. Patruno, IEEE Electron Device Lett. **27**, 120 (2006).
[12] S. C. Rustagi, N. Singh, Y. F. Lim, G. Zhang, S. Wang, G. Q. Lo, N. Balasubramanian, and D. -L. Kwong, IEEE Electron Device Lett. **28**, 909 (2007).
[13] S. Oda and D. Ferry, *Silicon Nanoelectronics* (Taylor & Francis, Boca Raton, 2006).
[14] J.-P. Colinge, Solid-State Electron. **51**, 1153 (2007).
[15] A. K. Buin, A. Verma, A. Svizhenko, and M. P. Anantram, Nano Lett. **8**, 760 (2008).
[16] C. Kittel and P. McEuen, *Introduction to Solid State Physics*, 8th ed. (Wiley, Hoboken, 2005).
[17] M. Lundstrom, *Fundamentals of Carrier Transport*, 2nd ed. (Cambridge University, Cambridge, 2000).
[18] J. Bardeen and W. Shockley, Phys. Rev. **80**, 72 (1950).
[19] M. S. Lundstrom and J. Guo, *Nanoscale Transistors: Device Physics, Modeling and Simulation* (Springer, New York, 2006).